JPhys Materials

Piezoelectric tunability and topological insulator transition in a GaN/InN/GaN quantum-well device

IOP Publishing J. Phys. Mater. 4 (2021) 034008 https://doi.org/10.1088/2515-7639/abf7dc

Journal of Physics: Materials

OPEN ACCESS

RECEIVED
9 December 2020

REVISED
1 March 2021

ACCEPTED FOR PUBLICATION
14 April 2021

PUBLISHED
28 April 2021

PAPER

Piezoelectric tunability and topological insulator transition in a GaN/InN/GaN quantum-well device

Daniele Barettin[1,*], Matthias Auf der Maur[2], Alessandro Pecchia[3], Yan Zhang[4,5], Morten Willatzen[5] and Zhong Lin Wang[5,6]

[1] UNICUSANO, Università degli Studi Niccolò Cusano—Telematica, Rome, Italy
[2] Department of Electronic Engineering, University of Rome 'Tor Vergata', Via del Politecnico 1, 00133 Rome, Italy
[3] CNR-ISMN, via Salaria Km. 29.300, 00017 Monterotondo, Rome, Italy
[4] School of Physics, School of Physical Electronics , University of Electronic Science and Technology of China, Chengdu, 610054, People's Republic of China
[5] Beijing Institute of Nanoenergy and Nanosystems, Chinese Academy of Sciences, National Center for Nanoscience and Technology (NCNST), Beijing 100083, People's Republic of China
[6] School of Material Science and Engineering, Georgia Institute of Technology, Atlanta, GA 30332, United States of America
[*] Author to whom any correspondence should be addressed.

E-mail: daniele.barettin@unicusano.it

Keywords: piezoelectric tunability, topological insulator transition, quantum-well device

Abstract

Using an 8-band $\mathbf{k}\cdot\mathbf{p}$ model it is demonstrated through the combination of strain and piezoelectricity that increasing the InN quantum-well thickness of a GaN-InN-GaN device changes the InN material from a positive bandgap semiconductor to a topological insulator (negative bandgap). Moderate strain tuning of a four monolayer InN layer for a GaN-InN-GaN device reveals a giant (one order of magnitude) tuning of current–voltage characteristics. It is verified that piezoelectricity plays an important role in controlling electron transport through the InN layer.

1. Introduction

Piezoelectricity [1–4] plays an important role in converting mechanical energy to electrical energy with applications in diverse fields such as ultrasonic transducers, cell phones, and vibration sensors. Ultrasonic transducers are key components in medical imaging and industrial transducer applications [5–8]. Zhong Lin Wang demonstrated in 2006 the principle and technological roadmap of nanogenerators harvesting mechanical energy from the environment and the use of biological systems for powering mobile sensors [9]. His group coined the fields of piezotronics and piezo-phototronics by showing how piezoelectric effects in nanostructures can make strain-gated transistors for new electronics, optoelectronics, sensors, and energy sciences [10].

With the discovery of graphene [11] and other 2D materials, the search for new materials with strong piezoelectricity and high flexibility has intensified [12, 13]. Another class of promising materials with interesting application potential is topological insulators (TI) where conduction and valence bands are inverted [14–21]. In this context, wurtzite GaN/InN quantum-well (QW) heterostructures represent a crucial case. In fact, a pressure-induced topological phase transition and the pressure evolution of topologically protected edge states in InN/GaN and In-rich InGaN/GaN QWs have been demonstrated in [22]. Realization of a topological phase transition and Rashba spin–orbit interaction in electrically biased InN/GaN QWs has been demonstrated in [23]. Furthermore, Miao and co-authors showed that polarization drives a TI transition in a GaN/InN/GaN QW structure [18]. Finally, transport properties of bulk and edge states as well as performances resembling those of TIs by a piezoelectric field in a GaN/InN/GaN QW device have been recently studied [24].

In the present work, based on the idea presented in [18], we use the effective piezoelectric tunable band inversion in a wurtzite GaN/InN QW heterostructures to show that the piezoelectric-controlled current density at a voltage of 1 V changes by a factor of 10 in the presence of a strain equal to -2.3%.

The paper is organized as follows. In section 2 the equation framework we have implemented for band structure, electromechanical fields, and transport calculations is presented. In section 3 we use 8-band $\mathbf{k}\cdot\mathbf{p}$ calculations to confirm effective bandgap control of GaN/InN QW heterostructures. Section 4 presents piezoelectric tunability due to a TI transition in a GaN/InN QW heterostructures with an applied bias. Finally, we give our conclusions.

2. Models

Bandstructure calculations are carried out using an 8-band wurtzite $\mathbf{k}\cdot\mathbf{p}$ Hamiltonian [25]. Electron, heavy-hole, light-hole, and spin–orbit split-off bands are described around the Γ point of the Brillouin zone while all other bands are treated as remote bands. The 8-band effective-mass Hamiltonian has been implemented using Foreman's application of Burt's exact envelope function theory to planar heterostructures [26]. Each wave function corresponding to a state n with energy E_n is given by a linear combination of eight Bloch states weighted by respective envelope functions,

$$\psi_n(r) = \sum_{i=1}^{8} \phi_n^i(r) u_{i\Gamma}(r), \tag{1}$$

with ϕ_n^i envelope functions and $u_{i\Gamma}$ Bloch states at $k = 0$ [27].

The electromechanical field that drives the system into the TI phase is calculated using a fully-coupled continuum model [28, 29].

Since wurtzite crystals exhibit a spontaneous polarization P_{sp} along the growth axis (in our model this is equivalent to the z axis), the components of the polarization are thus given by [30]:

$$\begin{aligned} P_x &= e_{15}\varepsilon_{xz}, \\ P_y &= e_{15}\varepsilon_{yz}, \\ P_z &= e_{31}(\varepsilon_{xx} + \varepsilon_{yy}) + e_{33}\varepsilon_{zz} + P_{sp}, \end{aligned} \tag{2}$$

where e_{il} is the position-dependent piezoelectric tensor and ε_{ik} is the position-dependent strain tensor.

The constitutive equations for the stress tensor σ_{ik} and the electrical displacement D_i are:

$$\begin{aligned} \sigma_{ik} &= c_{iklm}\varepsilon_{lm} - e_{ikn}\mathcal{E}_n, \\ D_i &= \epsilon_{in}\mathcal{E}_n + e_{ilm}\varepsilon_{lm} + P_{sp}, \end{aligned} \tag{3}$$

where c_{iklm}, ϵ_{in} and $\mathcal{E}_n$ are the position-dependent elastic modulus, the permittivity of the material and the electric field, respectively.

The Navier's static equations of motion and the Maxwell–Poisson equation are given by:

$$\begin{aligned} \frac{\partial \sigma_{ij}}{\partial x_j} &= 0, \\ \nabla \cdot D &= 0. \end{aligned} \tag{4}$$

From these we obtain a set of four coupled equations in the electromechanical fields.

Piezoelectric and strain fields have been included in $\vec{k}\cdot\vec{p}$ via deformation potentials [31] with parameters derived from [32, 33]. We consider pseudomorphic growth of InN on GaN where, due to the large strain misfit, InN values of deformation potentials are determined by first-principles calculations as described in [18, 34].

Carrier transport is simulated using a semi-classical drift-diffusion model. The electron and hole continuity equations coupled with the Poisson equation are solved using Newton's method. The full set of governing equations are discretized using the finite element method. Band edges and effective densities of states are obtained from bulk 8-band $\mathbf{k}\cdot\mathbf{p}$ calculations including Pikus–Bir strain corrections [31]. The local electric polarization, including spontaneous and piezoelectric contributions, is calculated from the local strain.

The calculated recombination rate R accounts for Shockley–Read–Hall (SRH) defect-mediated recombination, radiative recombination, and Auger recombination [35].

Transport of the carriers through the InN QW junction has been included by a trap-assisted transport model [36]. This model was introduced to describe a non-ideal forward current in heavily doped pn diodes [36, 37], and recently it has been applied to GaN pn junctions [38]. It is basically a conventional SRH recombination model with an electric-field dependent reduction of carrier lifetimes. The lifetime reduction

originates from an enhancement of carrier capture and emission rates at high electric fields because of phonon-assisted tunneling.

The SRH recombination rate for this model is given by:

$$R_{\text{trap}} = \frac{pn - n_i^2}{\frac{\tau_p}{1+\Gamma_p}(n + n_i e^{\frac{E}{kT}}) + \frac{\tau_n}{1+\Gamma_n}(p + n_i e^{-\frac{E}{kT}})}, \tag{5}$$

where $E = E_T - E_i$, is the difference between the trap level E_T and the intrinsic level E_i, n and p are the electron and hole densities, n_i is the intrinsic carrier concentration, τ_p and τ_n are the recombination lifetimes of electrons and holes, respectively, and finally Γ_p and Γ_n are field-effect functions [37]. For more model details, we refer to [39].

The transport, electro-mechanical and electronic models are implemented and solved using the TiberCAD [40–42] simulator.

3. Results for bandstructures of a GaN/InN/GaN well

It has been shown [18] for a system consisting of a thin InN well embedded in a GaN barrier that the band structure around the Γ point, calculated with density functional theory and a 6-band $\mathbf{k}\cdot\mathbf{p}$ effective model based on the 8-band $\mathbf{k}\cdot\mathbf{p}$ model (Kane model) for wurtzite semiconductors, exhibits a reduction of the effective bandgap and, eventually, an inversion of bands as the thickness of the well increases. This result has been considered one of the evidences of a transition to a TI state.

It is well known that for thin wells the bandgap between valence and conduction bands is influenced by three factors: quantum confinement, polarization field, and strain. Qualitatively, the quantum-confinement effect tends to increase the bandgap while the two other contributions tend to decrease the bandgap. The quantum confinement effect is predominant for very thin wells, i.e. for 1 or 2 InN monolayers (ML) characterized by bandgaps larger than for bulk InN. For more than 3 wells the bandgap contribution from quantum confinement is reduced to less than 0.1 eV in case of 3 or more ML [18]. On the other hand, the combined effect from spontaneous and piezoelectric polarizations results in a bandgap decrease. The three factors together lead to a gradual reduction of the bandgap at the Γ point as the thickness of the InN well increases.

Indeed this is confirmed by our results. In figure 1 we show 8-band $\mathbf{k}\cdot\mathbf{p}$ calculations for the band structure of a system consisting of an InN well embedded in a GaN matrix for 1, 4, and 6 ML (top to bottom plots). These results are used in the following section to compute transport properties.

We observe a qualitatively similar trend to those shown in [18], where it was demonstrated (figure 3(c)) that a TI transition indeed takes place. Compared to the bulk InN bandgap of 0.62 eV, the effective bandgap for a single ML of InN is about 2.3 eV due to the strong quantum confinement. The effective bandgap is reduced by polarization to about 0.3 eV in the case of 4 ML (medium panel) and nearly zero for 6 ML (bottom panel). This result, obtained in the framework of the 8-band $\mathbf{k}\cdot\mathbf{p}$ model, appears to confirm previous results [18].

4. Piezoelectric tunability in a GaN/InN/GaN quantum well

In order to demonstrate piezoelectric tunability due to a TI transition a simple device is modeled: a thin InN QW is inserted between a *p*–*n* junction. Both *p* and *n* regions consist of pure GaN with a concentration of donors and acceptors equal to $N_D = 10^{19}$ and $N_A = 5 \times 10^{19}$, respectively. Then, a positive bias from 0 to 1 *V* is applied to the *n*-side with respect to the *p*-side so as to have a reverse-biased *p*–*n* junction. The device is shown in figure 2.

In figure 3 we show the current density–voltage (*J*–*V*) characteristics for the device for 1, 4 and 6 ML.

At the same voltage we observe a >50% increase in the current density when going from 1 to 4 ML, and a roughly four-fold current density increase in the case of 6 ML. This effect is attributed to a significant increase in the transport of carriers due to narrowing of the bandgap. Our results confirm that the driving force behind this phenomenon is the piezoelectric effect. In fact, if simulations are carried out including the strain field but excluding the piezoelectric effect, three identical *J*–*V* characteristics (not shown here) result for 1, 4, and 6 ML.

As we have already mentioned in the Introduction, it has been shown that in a GaN/InN/GaN QW a thickness of 3 ML is the critical thickness for a TI transition [18, 23], and in this sense the 4 ML and the 6 ML configurations are both in a TI condition with zero gap. We therefore expect a very different physical situation for these latter cases compared to the case with 1 ML in terms of charge distribution. This can be seen in the insert of figure 3, where the electron densities for the three cases are shown. We observe that

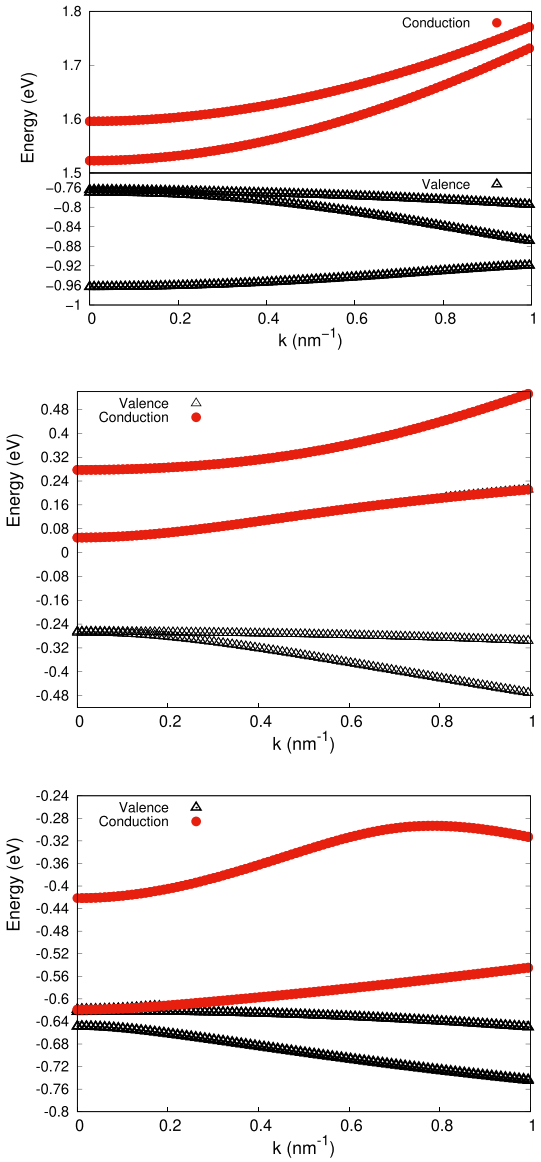

Figure 1. Bandstructure of a GaN/InN/GaN well for different thickness of the well: 1 ML (top), 4 ML (middle), 6 ML (bottom).

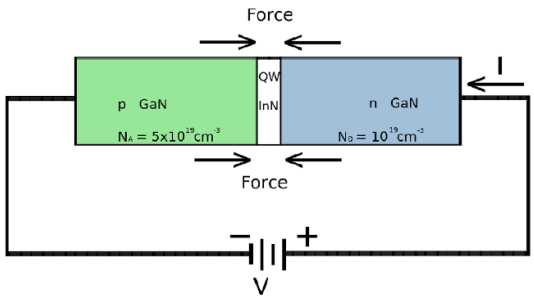

Figure 2. The device studied in our model: a GaN *p–n* junction with an inserted InN QW. The applied external mechanical force is along the *z* axis.

inside the well the density has approximately the same distribution for 4 and 6 ML, while it is more than five orders of magnitude lower in the case of 1 ML. This explains why, for this latter case, the current density is visibly lower and there is no piezoelectric tunability, as we will state later.

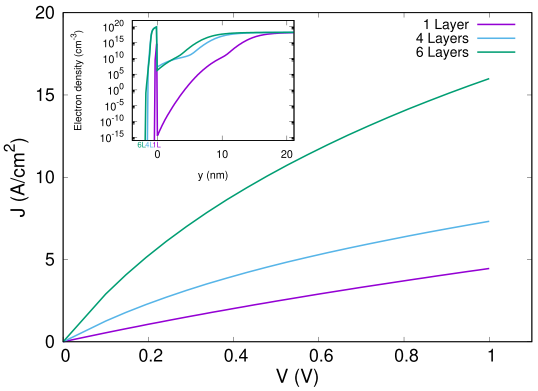

Figure 3. *J–V* characteristics of a GaN reverse-biased *p–n* junction with an inserted InN QW. Results are shown for three different thickness of the well. Inset: electron densities for the same cases.

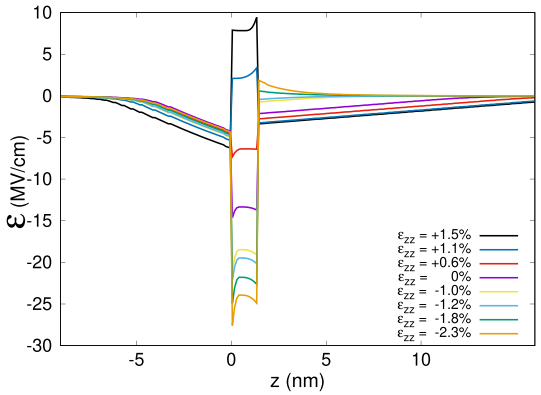

Figure 4. Electric field along the *z* axis for different values of applied strain.

Since the 4 and 6 ML cases present similar results in terms of piezoelectric tunability, in the following we discuss only the 4 ML InN case in detail, since this is a crucial thickness in the sense that for structures with smaller (larger) InN thicknesses the bandgap is positive (negative) for all the strain and bias cases considered.

Verified the onset of a transport effect linked to a transition to a TI state, a way to perform piezoelectric tunability in a wurtzite GaN/InN/GaN structure is by applying additional strain along the *z* axis. Such additional strain modifies the piezoelectric field as equations (4) reveal causing transitions between an insulator and a TI state [43].

Hence, with the application of external compressive or tensile mechanical force on the 4 ML-InN well of the device shown in figure 2, the intensity of the strain field as well as the electric field by virtue of the piezoelectric effect is modulated.

The electric field along the *z* direction is shown in figure 4 for different values of the applied strain component ε_{zz}. We observe that a decrease (increase) of the ε_{zz} strain component strengthens (attenuates) the electric field. For a sufficiently high ε_{zz} value the electric field changes sign.

A direct consequence of the variation of the electric field on electronic bandstructures is shown in figure 5 for three different applied strain values: $\varepsilon_{zz} = 0\%$, $\varepsilon_{zz} = 2.3\%$, and $\varepsilon_{zz} = +1.5\%$.

In all three situations, a quasi-zero gap condition occurs revealing a TI transition. Note, however, that the slope of the bands are significantly different for the three strain cases. The slope of the conduction and valence bands along the growth direction in wurtzite structures is a consequence of the quantum-confined Stark effect, i.e. the electric field along the growth axis of the crystal [44, 45]. The transport of carriers increases sharply with the increase of the electric field in the InN layer and explains why the case with an external strain of -2.3% leads to the highest current density at a given bias. It should be pointed out that the limiting factor for the maximum current density output is the value of the strain the device can withstand before defects are introduced.

This is indeed confirmed by figure 6 where *J–V* characteristics for different values of ε_{zz} are shown (4 ML InN case). Observe that the current flow increases by a factor of 10 for the case with -2.3% strain compared

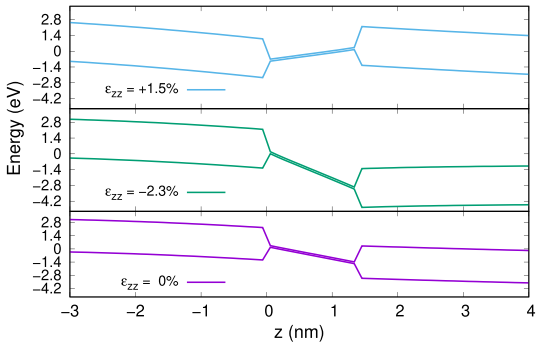

Figure 5. Conduction and valence bands vs. z direction for three values of the ε_{zz} applied strain component: 0% (bottom), −2.3% (central), and +1.5% (top).

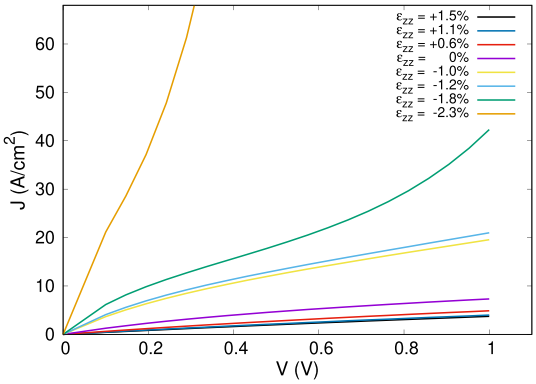

Figure 6. $J-V$ characteristics of a GaN reverse-biased p–n junction with in between a 4 ML InN QW for different values of the ε_{zz} applied strain component.

to the unstrained case. Notice also that inversion of the electric field, corresponding to $\varepsilon_{zz} = +1.5\%$, effectively diminishes current flow through the device.

In order to verify that our results are strictly related to a TI phase transition, and not simply to the presence either of an induced piezoelectric field or an applied strain, we carried out three benchmark simulations, all with an applied strain of −1.8%.

In the first simulation we replaced the 4 ML InN QW with an undoped 4 ML GaN QW. Despite the application of a strain and consequently the presence of a polarization, the J–V curves did not change significantly in the presence of external strain.

In the second case we have reduced the 4 ML InN QW to a 1 ML InN QW. The effect on the J–V characteristics is practically negligible, showing that if the junction is in the insulating phase (positive gap) the system is not suitable for piezoelectric tunability.

Finally, we have increased the 4 ML InN QW up to 6 ML InN QW. In this case we observe the same effect shown in figure 6, even more intensely. This was predictable, as in this case we know the junction to be in a TI phase. We do think that the determination of the optimal junction thickness has to be determined experimentally.

By changing the external strain from 0 to −2.3%, we obtain a shift in dJ/dV by a factor of about 20 for voltages in the range 0–0.2 V which is considerably higher than those reported for piezoelectric ZnO p–n junction nanowires (where dJ/dV changes by a factor of about 3) in [10, 46].

In [18], it is demonstrated using DFT and an effective 6-band $\mathbf{k}\cdot\mathbf{p}$ model that piezoelectric effects in GaN-InN-GaN structures lead to an inverted bandstructure when the InN layer number is above 5 (from $\mathbf{k}\cdot\mathbf{p}$) by virtue of the lattice mismatch strain. In the present work, we confirm the results of [18]. using an 8-band $\mathbf{k}\cdot\mathbf{p}$ model and then go on to demonstrate piezoelectric tuning of J–V curves via external strain. We obtain a giant piezoelectric tuning range of dJ/dV in a broad voltage region via external strain due to a transition of the InN QW layer from a normal semiconductor to a TI state.

We point to that besides the current computed above, a net spin edge current may supervene when external strain tunes the InN layer into the TI state. This spin edge current is not considered in our work. We anticipate further theoretical investigations and experimental results on piezoelectric strain tuning, attaining

a transition from a normal semiconductor to a TI state, will clarify the potential of the present idea for device applications.

5. Conclusions

A device consisting of p–n GaN structure with an inserted InN QW layer is analyzed in terms of current–voltage characteristics and piezoelectric tuning. We first demonstrate using an 8-band $\mathbf{k}\cdot\mathbf{p}$ model that the InN QW layer thickness is crucial for converting the GaN/InN/GaN structure into a topological state. It is also demonstrated that the competing effects of quantum confinement vs. spontaneous polarization and piezoelectricity determine the onset of the TI effect as a function of the InN well thickness. For very thin InN layers (less than 4 ML) the quantum confinement effect dominates resulting in a positive InN bandgap. For an InN thickness of 6 ML or above the bandgap is inverted (topological state). It is shown that the piezoelectric effect is the determining factor for the magnitude and direction of the electric field in the InN layer and, hence, transport properties. As a result, a sufficiently large negative applied strain component ($\varepsilon_{zz} = -2.3\%$) leads to an increase by a factor of 10 in the current density for a given bias voltage by virtue of the piezoelectric effect.

Data availability statement

The data that support the findings of this study are available upon reasonable request from the authors.

Acknowledgments

D B acknowledges financial support and hospitality from Beijing Institute of Nanoenergy and Nanosystems, Chinese Academy of Sciences. M W acknowledges financial support from a Talent 1000 Program for Foreign Experts.

ORCID iDs

Daniele Barettin https://orcid.org/0000-0002-2849-1898
Matthias Auf der Maur https://orcid.org/0000-0002-4815-4485
Morten Willatzen https://orcid.org/0000-0002-8215-9650

References

[1] Mason W P 1948 *Electromechanical Transducers and Wave Filters* 2nd edn (New York: Van Nostrand Company, Inc.)
[2] Redwood M 1961 *J. Acoust. Soc. Am.* **33** 527
[3] Desilets C S, Fraser J D and Kino G S 1978 *IEEE Trans. Son. Ultrason.* **SU-25** 115
[4] Goll J and Auld B A 1975 *IEEE Trans. Son. Ultrason.* **SU-22** 53
[5] Kino G S 1987 *Acoustic Waves, Devices, Imaging and Analog Signal Processing* (Englewood Cliffs, NJ: Prentice-Hall)
[6] Jensen J A 1996 *Estimation of Blood Velocities Using Ultrasound—A Signal Processing Approach* (New York: Cambridge University Press)
[7] Delsing J 1987 *IEEE Trans. Ultrason., Ferroelec. Freq. Control UFFC-34* p 431
[8] Willatzen M 2001 *IEEE Trans. Ultrason., Ferroelec. Freq. Control UFFC-48* p 100
[9] Wang Z L and Song J 2006 *Science* **312** 242
[10] Wang Z L 2012 *Piezotronics and Piezo-Phototronics* 1st edn (Berlin: Springer)
[11] Novoselov K S, Geim A K, Morozov S V, Jiang D, Zhang Y, Dubonos S V, Grigorieva I V and Firsov A A 2004 *Science* **306** 666
[12] Michel K H and Verberck B 2009 *Phys. Rev.* B **80** 224301
[13] Duerloo K A N, Ong M T and Reed E J 2012 *J. Phys. Chem. Lett.* **3** 2871
[14] Kane C L and Mele E J 2005 *Phys. Rev. Lett.* **95** 226801
[15] Kane C L and Mele E J 2005 *Phys. Rev. Lett.* **95** 146802
[16] Bernevig B A, Hughes T L and Zhang S-C 2006 *Science* **314** 1757
[17] Zhang H, Liu C, Qi X, Dai X, Fang Z and Zhang S 2009 *Nat. Phys.* **5** 438
[18] Miao M S, Yan Q, Van de Walle C G, Lou W K, Li L L and Chang K 2012 *Phys. Rev. Lett.* **109** 186803
[19] Zhang D, Lou W, Miao M, Zhang S-C and Chang K 2013 *Phys. Rev. Lett.* **111** 156402
[20] Wu W *et al* 2014 *Nature* **514** 470
[21] Rosdahl Brems M, Paaske J, Lunde A M and Willatzen M 2018 Strain-enhanced optical absorbance of topological insulator films *Phys. Rev.* B **97** 081402(R)
[22] Łepkowski S P and Bardyszewski W 2017 Topological phase transition and evolution of edge states in In-rich InGaN/GaN quantum wells under hydrostatic pressure *J. Phys. Condens. Matter* **29** 055702
[23] Łepkowski S P and Bardyszewski W 2017 Anomalous Rashba spin–orbit interaction in electrically controlled topological insulator based on InN/GaN quantum wells *J. Phys. Condens. Matter* **29** 195702
[24] Dan M, Hu G, Li L and Zhang Y 2018 High performance piezotronic logic nanodevices based on GaN/InN/GaN topological insulator *Nano Energy* **50** 544
[25] Lew Yan Voon L C and Willatzen M 2009 *Thek · pMethod: Electronic Properties of Semiconductors* (Berlin: Springer)

[26] Foreman B A 1993 *Phys. Rev.* B **48** 4964
[27] Pokatilov E P, Fonoberov V A, Fomin V M and Devreese J T 2001 *Phys. Rev.* B **64** 245328
[28] Barettin D, Madsen S, Lassen B and Willatzen M 2012 *Commun. Comput. Phys.* **11** 797
[29] Barettin D D, Lassen B and Willatzen M 2008 *J. Phys.: Conf. Ser.* **107** 012001
[30] Barettin D, Madsen S, Lassen B and Willatzen M 2010 *Superlattices Microstruct.* **47** 134
[31] Bir G L and Pikus G E 1974 *Symmetry and Strain-Induced Effects in Semiconductors* (New York: Wiley) p 295
[32] Vurgaftman I, Meyer J R and Ram-Mohan L R 2001 *J. Appl. Phys.* **89** 5815
[33] Vurgaftman I and Meyer J R 2003 *J. Appl. Phys.* **94** 3675
[34] Yan Q, Rinke P, Scheffler M and Van de Walle C G 2009 *Appl. Phys. Lett.* **95** 121111
[35] Schiavon D, Binder M, Peter M, Galler B, Drechsel P and Scholz F 2013 *Phys. Status Solidi* b **250** 283
[36] Hurkx G, Klaassen D, Knuvers M and O'Hara F 1989 *Tech. Dig.—Int. Electron Devices Meet.* vol 307
[37] Hurkx G, Klaassen D and Knuvers M 1992 *IEEE Trans. Electron Devices* **39** 331
[38] Sakowski K, Marcinkowski L, Krukowski S, Grzanka S and Litwin-Staszewska E 2012 *J. Appl. Phys.* **111** 123115
[39] Auf der Maur M, Galler B, Pietzonka I, Strassburg M, Lugauer H and Di Carlo A 2014 *Appl. Phys. Lett.* **105** 133504
[40] TiberCAD Simulation Package (available at: http://www.tibercad.org)
[41] Barettin D, De Angelis R, Prosposito P, Auf der Maur M, Casalboni M and Pecchia A 2015 *J. Appl. Phys.* **117** 9
[42] Barettin D, De Angelis R, Prosposito P, Auf der Maur M, Casalboni M and Pecchia A 2014 *Nanotechnology* **25** 195201
[43] Hu G, Zhang Y, Li L and Wang Z L 2018 *ACS Nano* **12** 779
[44] Waltereit P, Brandt O, Trampert A, Grahn H T, Menniger J, Ramsteiner M, Reiche M and Ploog K H 2000 *Nature* **406** 865
[45] Barettin D *et al* 2017 *Nanotechnology* **28** 015701
[46] Zhang Y, Yang Y and Wang Z L 2012 *Energy Environ. Sci.* **5** 6850–6